CHEMMEDCHEM

CHEMISTRY ENABLING DRUG DISCOVERY

Accepted Article

Title: Binding Mode and Structure-Activity Relationships of ITE as Aryl Hydrocarbon Receptor (AhR) Agonist.

Authors: Daniela Dolciami, Marco Gargaro, Bruno Cerra, Giulia Scalisi, Luana Bagnoli, Giuseppe Servillo, Maria Agnese Della Fazia, Paolo Puccetti, Francisco J Quintana, Francesca Fallarino, and Antonio Macchiarulo

To be cited as: *ChemMedChem* 10.1002/cmdc.201700669

Link to VoR: http://dx.doi.org/10.1002/cmdc.201700669

A Journal of

ChemPubSoc Europe

WILEY-VCH

www.chemmedchem.org

WILEY-VCH

FULL PAPER

Binding Mode and Structure-Activity Relationships of ITE as Aryl Hydrocarbon Receptor (AhR) Agonist.

Dr. Daniela Dolciami,[a, e] Dr. Marco Gargaro,[b, e] Dr. Bruno Cerra,[a] Dr. Giulia Scalisi,[b] Dr. Luana Bagnoli,[a] Dr. Giuseppe Servillo,[b] Dr. Maria Agnese Della Fazia,[b] Prof. Paolo Puccetti,[b] Prof. Francisco J. Quintana,[c, d] Prof. Francesca Fallarino,[b] Prof. Antonio Macchiarulo.*[a]

[a] Dr. Daniela Dolciami, Dr. Bruno Cerra, Dr. Luana Bagnoli, Prof. Antonio Macchiarulo.
Department of Pharmaceutical Sciences,
University of Perugia,
via del Liceo, 1 - 06123, Perugia (Italy).
E-mail: antonio.macchiarulo@unipg.it

[b] Dr. Marco Gargaro, Dr. Giulia Scalisi, Dr. Giuseppe Servillo, Dr. Maria Agnese Della Fazia, Prof. Paolo Puccetti, Prof. Francesca Fallarino,
Department of Experimental Medicine,
University of Perugia,
via Gambuli, 1 – 06132, Perugia (Italy).

[c] Prof. Francisco J. Quintana,
Ann Romney Center for Neurologic Diseases, Brigham and Women's Hospital,
Harvard Medical School,
Boston (USA).

[d] Prof. Francisco J. Quintana,
The Broad Institute of Harvard and MIT,
Cambridge (USA).

[e] These authors contributed equally to the work.

Supporting information for this article is given via a link at the end of the document.

Abstract: Discovered as modulator of the toxic response to environmental pollutants, aryl hydrocarbon receptor (AhR) has recently gained attention for its involvement in various physiological and pathological pathways. AhR is a ligand-dependent transcription factor activated by a large array of chemical compounds, which include metabolites of L-Tryptophan (L-Trp) catabolism as endogenous ligands of the receptor. Among these, 2-(1'H-indole-3'-carbonyl)-thiazole-4-carboxylic acid methyl ester (ITE) is attracting interest in the scientific community, being endowed with non-toxic, immunomodulatory and anticancer AhR-mediated functions. So far, no information about the binding mode and interactions of ITE to AhR is available. In this study, we used docking and molecular dynamics to propose a putative binding mode of ITE into the ligand binding pocket of AhR. Mutagenesis studies were then instrumental to validate the proposed binding mode, identifying His285 and Tyr316 as important key residues for ligand-dependent receptor activation. Finally, a set of ITE analogues was synthesized and tested to further probe molecular interactions of ITE to AhR, and characterize the relevance of specific functional groups in the chemical structure for receptor activity.

Introduction

Aryl hydrocarbon Receptor (AhR) is a ligand-activated transcription factor known for its involvement in human responses to environmental pollutants such as 2,3,7,8-tetrachlorodibenzo-*p*-dioxin (TCDD, **1**; Figure 1). In addition to this extensively characterized role in detoxification of xenobiotic, during the last few years the role of AhR in other physiologically and pathologically relevant pathways have been reported, including regulation of stem cells, embryogenesis, immune functions, inflammation and carcinogenesis.[1,2] Many exogenous compounds possessing different physicochemical properties, for example halogenated aromatic hydrocarbons (HAHs) and polycyclic aromatic hydrocarbons (PAHs), act as AhR agonists. Recently, some natural products have also been characterized as AhR ligands, including the bacterial-derived metabolite 1,4-dihydroxy-2-naphthoic acid (1,4-DHNA, **2**),[3] and products of L-Tryptophan (L-Trp) catabolism comprising L-Kynurenine (L-Kyn, **3**), ICZ (indolo[3,2-b]carbazole, **4**), FICZ (6-formylindolo[3,2-b]carbazole, **5**), malassezin (**6**), and ITE (2-(1'*H*-indole-3'-carbonyl)-thiazole-4-carboxylic acid methyl ester, **7**) (Figure 1).[4-7] In particular, ITE (**7**) was isolated from porcine lung in 2002 and it has been reported as a high affinity AhR ligand (Ki = 3nM) being able to compete with ^{3}H-TCDD for binding to human, murine, zebrafish and killifish isoforms of the receptor. The agonistic activity of **7** is blocked by the AhR antagonist 3'-methoxy-4'-nitroflavone (**8**; Figure 1).[6]

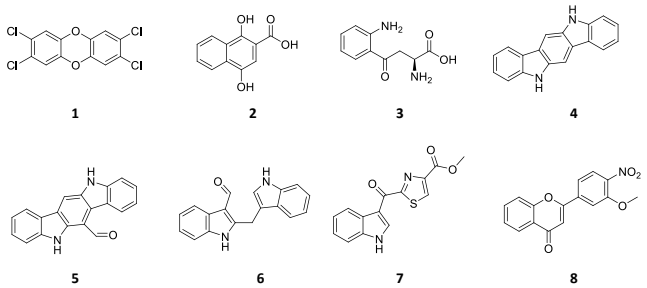

Figure 1. AhR modulators. TCDD, **1**; 1,4-DHNA, **2**; L-Kynurenine, **3**; ICZ, **4**, FICZ, **5**; malassezin, **6;** ITE, **7**; 3'methoxy-4'-nitroflavone, **8**.

Pharmacological studies have pinpointed both immunosuppressive and anticancer functions of ITE (**4**) that are mediated by the activation of AhR. Specifically, ITE (**7**) is able to induce functional FoxP3^{+} Treg cells, leading to immunosuppressive effects in a model of experimental autoimmune encephalomyelitis (EAE).[8] Immunomodulatory effects of ITE (**7**) have also been observed in a model of

experimental autoimmune uveitis (EAU) in response to uveitogenic antigen.[9] Moreover, ITE (**5**)-induced AhR activation has been reported to inhibit the expression of co-stimulatory molecules and secretion of cytokines by dendritic cells (DCs) from mice,[8] and also from Behcet's disease (DRE) patients.[10] Likewise, AhR activation has been shown to inhibit Th17 inflammatory response, regulating both DCs and CD4(+) T cells derived from patients with allergic rhinitis.[11] Besides affecting differentiation and functions of Th17/Treg cells, additional AhR mediated immunological effects of ITE (**7**) have emerged, specifically the ability of the compound to suppress B cells differentiation into Ig-secreting plasma cells.[12] AhR mediated anticancer activities of ITE (**7**) have also been reported including the suppression of proliferation and migration of ovarian cancer cells,[13] and the reduction of the tumorigenic potential of stem-like cancer cells in orthotopic xenograft tumor models.[14]

Noteworthy, the above immune regulatory and anticancer functions of ITE (**7**) combine with lack of significant toxicity, a finding at odds with the toxicity of other potent AhR agonists such as TCDD (**1**). Notably, ITE-activated AhR forms a transcriptionally competent complex which binds to Dioxin Responsive Elements (DRE) similarly to TCCD-activated AhR, however ITE does not provoke toxic effects in rat and mouse fetus.[15,16]

As an attempt to provide an explanation to the divergent toxicity of ITE (**7**) and TCDD (**1**), a recent study surprisingly pinpointed that these ligands regulate similar immediate changes in gene expression in mouse lung fibroblasts.[17] Accordingly, ITE (**7**) and TCDD (**1**) bind to PAS-B (PER-ARNT-SIM-B) domain of AhR, triggering analogous conformational changes of the receptor that lead to the same initial transcriptional response. Hence, authors suggested that the lack of toxicity of ITE (**7**) may be ascribed to its ability to form a shorter life-time complex with the receptor than that induced by TCDD (**1**), resulting in different kinetics of gene expression.[17] Although no crystallographic information exists on the structural complex between ITE (**7**) and AhR that may be instrumental to infer about different binding modes of ITE (**7**) and TCDD (**1**), previous docking studies into homology models suggested that both ligands may adopt a similar binding mode to PER-ARNT-SIM-B domain (PAS-B) of the receptor.[18,19]

More recently, we have shown that TCDD (**1**) and two other different L-Trp metabolites, namely L-Kyn (**3**) and FICZ (**5**), bind to PAS-B of AhR exploiting different key interactions with distinct set of fingerprint residues.[20] The outcome is the stabilization of different conformations of the receptor associated to the transcription of specific target genes.

With the aim of shedding further light on the binding mode of ITE (**7**) to AhR and assessing potential difference from TCDD (**1**), in this work we investigate the interaction of ITE (**7**) to PAS-B domain by integrating an approach composed of computational studies, mutagenesis experiments and synthesis of ITE analogues. Specifically, in the first part of the study we have performed docking and molecular dynamic (MD) simulations to generate a prospective working hypothesis on the binding mode of ITE (**7**) to PAS-B domain of AhR. Results instrumental for designing mutagenesis experiments on proposed fingerprint residues for ITE were validated by AhR-specific gene reporter transcription assays. Finally, a set of ITE analogues were designed, synthetized and tested to further probe molecular interactions of ITE to AhR and characterize the relevance of specific functional groups in the chemical structure for receptor activity.

Results and Discussion

Docking Study and Molecular Dynamics. Docking studies and MD simulations were instrumental to characterize the interaction pattern of ITE (**7**) to PAS-B domain of AhR. Using our previously generated homology models of murine PAS-B AhR (**a-d**),[20] ITE (**7**) was docked into each of the four models. Briefly, the four models of PAS-B AhR feature different properties of the ligand binding cleft. The ligand binding cavities of model **a** and **c** have a small size with hydrophobic properties; the binding clefts of model **b** and **d** are large and display hydrophilic properties. Hence, each of the four models of PAS-B AhR represents a specific conformation of the ligand binding cavity that may accommodate ligands with different physicochemical properties. In order to improve the reliability of the energy scoring function by better considering dispersion forces of hydrophobic and/or π-π stacking interactions, docking studies were conducted using a method incorporating quantum mechanical/molecular mechanical (QM/MM) calculations.[21]

As a result, ITE (**7**) shows the best energy score (XP-Gscore = -8.421kcal/mol; Table S1 of supplementary material) when docked into model **d** which is endowed with the most pronounced hydrophilic features. This docked pose shows a hydrogen bond mediated engagement of Tyr316 by the carbonyl group of ITE (**7**), and the presence of aromatic contacts between the thiazole moiety and the side chain of His285 as well as hydrophobic and/or aromatic contacts between the indole ring and side chains of Phe318 and Tyr304 (Figure 2). It should be mentioned that alternative binding poses may be envisaged in the remaining docking solutions of models **a**-**d**, with RMSD > 2.0 Å from the top scored binding pose of ITE (Table S1, Figures S1-S7).

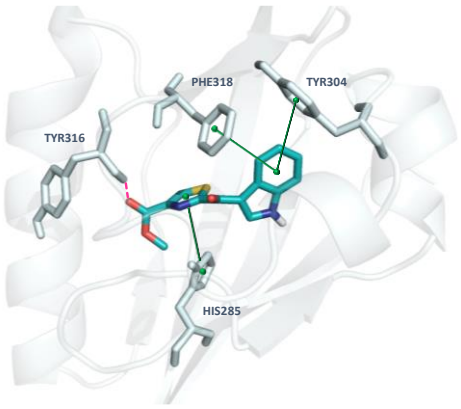

Figure 2. ITE best docking pose in model **d**. The most important residues for the interaction are represented in sticks. Green lines indicate π-π stacking interactions, whereas dashed pink line stands for H-bond.

Although scoring functions have been generally considered problematic at distinguishing the crystallographic conformation from the set of docked poses,[22] improvements obtained by incorporating QM/MM calculations prompted us to select the aforementioned top ranked pose of ITE (**7**) as working hypothesis of binding mode for MD simulations, according to a criteria of best energy score.[23-25] This docked pose was thus submitted to six independent runs of 50 ns MD simulations in order to assess the stability of the interactions and identify fingerprint residues. The inspection of the root mean square deviation (RMSD) of protein

backbone atoms reveals a stabilization of the complex after the first 10 ns in all MD simulations (Figure 3).

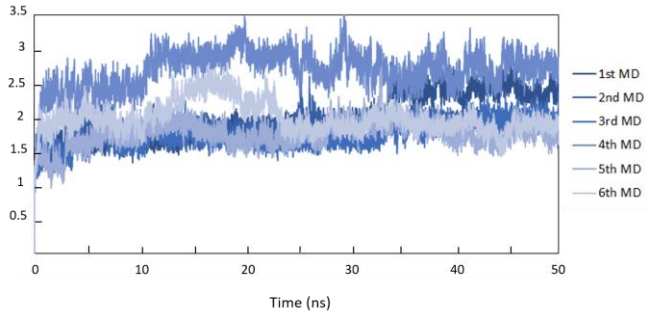

Figure 3. RMSD (Root Mean Square Deviation) values (Å) of protein backbone atoms along molecular dynamic trajectories.

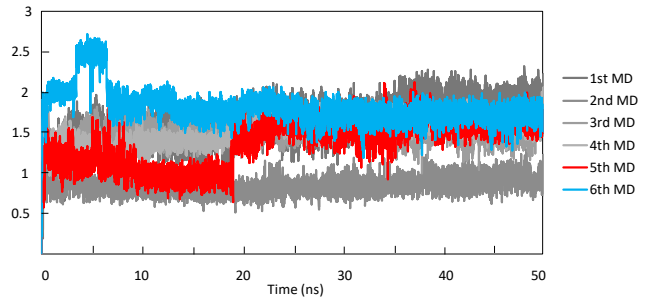

Figure 4. RMSD values (Å) of ITE atoms along molecular dynamic trajectories.

In the first simulation, the RMSD value undergoes to an increase around the 35th ns and then remains stable until the end of the simulation. In the fourth simulation, which is the one reaching the highest value of RMSD, a jump around 10th ns is detectable. Moreover, in the sixth simulation, the complex undergoes to a RMSD jump between 15th and 25th ns and then returns to lower drifts. To assess whether these movements affect the docked pose, the RMSD of ITE (**7**) and root mean square fluctuations (RMSF) of residues lying in a shell of 3Å around the ligand docked pose were calculated along the trajectories. Examining the RMSD plot (Figure 4), significant jumps of ligand are detectable in the fifth and sixth simulations. Specifically, the jump around the 20th ns of the fifth MD simulation is linked to rotational and translational movements of the entire ligand within the binding pocket, as exemplified in Figure 5A.

Conversely, the large drifts during the first five nanoseconds of the sixth MD are ascribed to torsional movements of the indole moiety (Figure 5B).

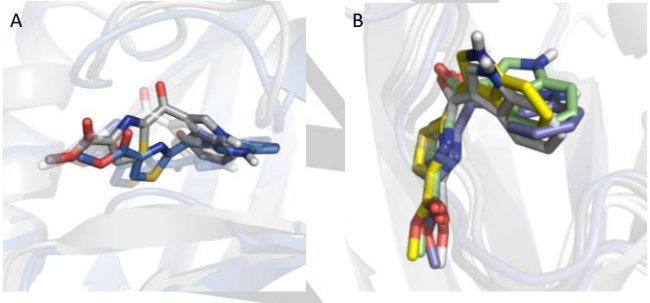

Figure 5. (**A**) Rotational and translational movements of ITE (**7**) during the 5th MD simulation. (**B**) Translational movement of ITE (**7**) during the 6th MD simulation.

The inspection of root mean square fluctuations of residues (RMSF; Table S2, supplementary material) suggests that conformations of most residues within 3Å of the ligand docked pose are generally stable, with only Leu309, Gly315 and Tyr316 showing RMSF > 1.5 Å in at least one MD simulation. In particular, these conformational drifts may suggest the engagement of ITE (**7**) with additional hydrophobic and aromatic interactions by the side chains of Leu309 and Tyr316, and/or with the optimization of hydrogen bond interactions involving the backbone atoms of such residues.

Next, we defined putative fingerprint residues of ITE (**7**) as those yielding average values of ligand interaction occupancy higher than 0.3 in all MD trajectories. Accordingly, the following potential fingerprint residues were identified in MD simulations: His285, Tyr316 and Phe318 (Table S3, supplementary material).

Specifically, Phe318 makes a hydrogen bond between its backbone amide group and ITE carbonyl group (Figures 6A-D), that may also be stabilized by mean of a water bridge interaction (as observed in the first MD simulation, Figure 6A). Notwithstanding, contribution of such interactions to the agonist activity of ITE (**7**) may be negligible, as suggested by indirect evidences from structure-activity relationship studies of another L-Trp metabolite, namely malassezin (**6**).[26]

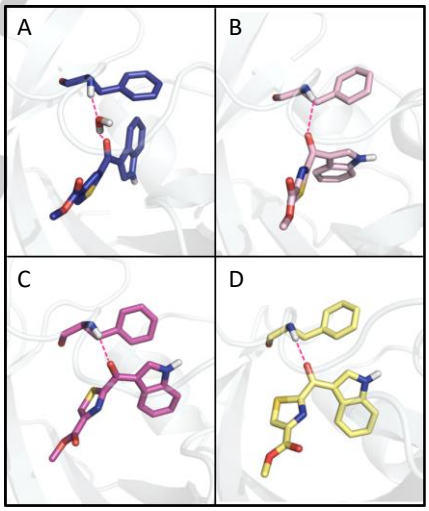

Figure 6. Crucial interactions of Phe318 with ITE (**7**) during MD simulations. Phe318 is involved in Hydrogen bond with carbonyl group of ITE, in one case mediated by a water bridge. (**A**) 1st MD simulation. (**B**) 2nd MD simulation. (**C**) 3rd MD simulation. (**D**) 6th MD simulation.

Tyr316 makes a hydrogen bond between its backbone amide group and ITE carbonyl oxygen (as observed in the first MD simulation, Figure 7A) or with the nitrogen atom of the thiazole ring of ITE (**7**) (as observed in the second and fifth MD simulations, Figure 7B, C), being this latter also stabilized by means of water bridges (as observed in the sixth MD simulation, Figure 7D).

His285 is involved in a π-π stacking aromatic interaction with the thiazole ring (as observed in the second and fifth MD simulation, Figure 8A, B) or alternatively with the indole ring of ITE (as observed in the sixth MD simulation, Figure 8C). The same residue makes a hydrogen bond interaction through a water bridge with the nitrogen atom of the thiazole ring of ITE (as observed in the sixth MD simulation, Figure 8D). Of note, no hydrogen bond interaction was observed between ITE (**7**) and Ser359, as previously reported from other docking studies.[18,19]

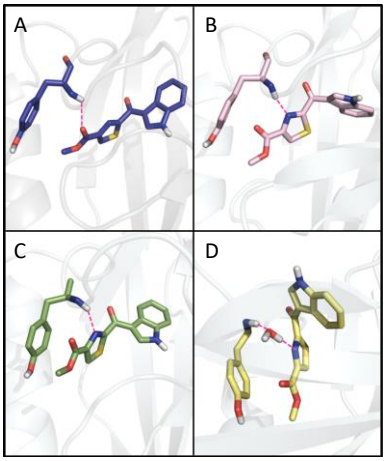

Figure 7. Crucial interactions of Tyr316 with ITE (**7**) during MD simulations. Tyr316 is involved in Hydrogen bond with Nitrogen atom of thiazole ring, in one case mediated by a water bridge. In the 1st MD, Tyr316 binds carbonyl group of ester moiety. (**A**) 1st MD simulation. (**B**) 2nd MD simulation. (**C**) 5th MD simulation. (**D**) 6th MD simulation.

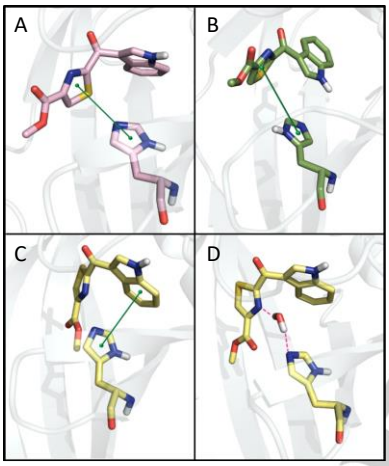

Figure 8. Crucial interactions of His285 with ITE (**7**) during MD simulations. His285 is mostly involved in π-π stacking interaction with thiazole or indole rings. In the 6th MD, His285 interacts by means of a water bridge with Nitrogen atom of thiazole ring. (**A**) 2nd MD simulation. (**B**) 5th MD simulation. (**C**) 6th MD simulation. (**D**) 6th MD simulation.

Mutagenesis experiments. On the basis of the results of docking study and MD simulations of ITE (**7**), two mutant AhR receptors were engineered carrying His285Ala mutation (H285A) and Tyr316Ala mutation (Y316A). It is worth noting that residue Gln377 was formerly identified as important in mediating a key hydrogen bond interaction with L-Kyn (**3**), but not involved in interactions with TCDD (**1**) and FICZ (**5**).[20] Residue Gln377 does not fall within 3Å of ITE docked pose, and shows only a weak hydrogen bond interaction with the ligand in one simulation (fourth MD simulation, average occupancy value of 0.19 ± 0.20). Notwithstanding, a third mutant receptor was designed bearing Gln377Ala mutation (Q377A) to probe by mutagenesis the role of such polar residue in mediating ITE (**7**) activity. To explore the impact of specific amino acid residues in ITE-induced AhR activation we established mouse embryonic fibroblast from AhR deficient mice (MEF $AhR^{-/-}$). Thus, MEF $AhR^{-/-}$ were reconstituted with AhR^{WT} or AhR^{H285A}, or AhR^{Y316A}, or AhR^{Q377A}. Transfection efficiency was similar for the four constructs, as revealed by western blot analysis on cell protein lysates (Figure 9A).

When assayed in a luciferase reporter assay using mouse DCs reconstituted with mutated AhR^{H285A} or AhR^{Y316A}, ITE (**7**) exhibits a complete loss of biologic activity, in terms of potency and likely affinity, compared to AhR^{WT} transfected counterpart (Figure 9B). In contrast, only a minor and negligible decrease of transactivation activity is observed when ITE (**7**) is tested in MEF reconstituted with AhR^{Q377A}, suggesting a slightly lower affinity of the ligand at this mutant receptor. Hence, mutagenesis experiments support the role of His285 and Tyr316 as fingerprint residues of ITE (**7**), highlighting poor relevance of Gln377 for ligand activity.

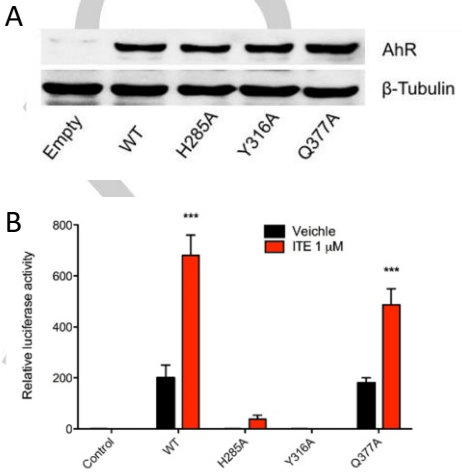

Figure 9. (A) AhR expression in MEF transfected with WT or H285A, Y316A, G377A AhR mutants. AhR-deficient mouse embrional fibrobasts (MEF) were transfected with WT or different AhR mutants: AhR(H285A), AhR(Q377A), AhR(Y316A) or AhR(Y316A/Q377A). After 24 h, cells were lysed, and analysed for AhR expression by immunoblotting, using a specific AhR antibody. β-tubulin was used as a loading control. Data are from one experiment of three. **(B)** Transactivation activity of WT, H285A, Y316A or G377A AhR by ITE (**7**). AhR-deficient mouse embrional fibrobasts (MEF) were transfected with WT or different AhR mutants: AhR(H285A), AhR(Q377A), AhR(Y316A) or AhR(Y316A/Q377A). After 6 h, cells were lysed, and the amount of AhR–ARNT–DRE complex was achieved by measuring luciferase activity. Data mean ± s.d. of three independent experiments. ***p ≤ 0.001 as determined by a Student's t test.

Design, Synthesis and Structure-Activity Relationships of ITE Analogues. Docking study and MD simulations have evidenced hydrophobic contacts (Phe289, Leu309, Phe318), π-π stacking aromatic interactions (His285, Phe289, Tyr316, Phe318), and hydrogen bonds (His285, Thr283, Leu309, Tyr316, Phe318) as involved in the stabilization of ITE (**7**) binding to PAS-B AhR. Among the proposed fingerprint residues, mutagenesis experiments have proved the importance of His285 and Tyr316 for the transcriptional activity of ITE (**7**), and likely for the affinity of ligand to the receptor. These residues, however, are involved in different kinds of interaction with specific pharmacophoric groups of ITE (**7**), depending on the trajectory that is analyzed out of the six MD simulations. Specifically, His285 is involved in a π-π stacking aromatic interaction with the indole ring or the thiazole moiety of ITE (**7**). A water mediated hydrogen bond is also observed in a trajectory between His285 and the nitrogen atom of the thiazole ring. Likewise, hydrogen bonds are observed between the backbone atoms of Tyr316 and the ester group or thiazole ring of the ligand.

Overall, these observations suggest that the thiazole moiety of ITE (**7**) may be an important pharmacophoric group promoting key aromatic and/or hydrogen bond interactions within the ligand binding pocket of PAS-B AhR. To further investigate the relevance of the thiazole moiety and its interactions to PAS-B AhR, a set of ITE (**7**) analogues were designed, synthetized and tested using the specific AhR reporter hepatic H1L1 cells (Figure 10). Specifically, compound **9** was conceived to bear a biososteric replacement of the thiazole ring with an oxazole ring, keeping the aromatic feature of this moiety while increasing its polarity (clogP = 1.60, table 1). In compound **10**, the aromatic feature of the central heterocycle was removed to assess the importance of the π-π stacking interaction of this moiety to the receptor with respect to compound **9**.

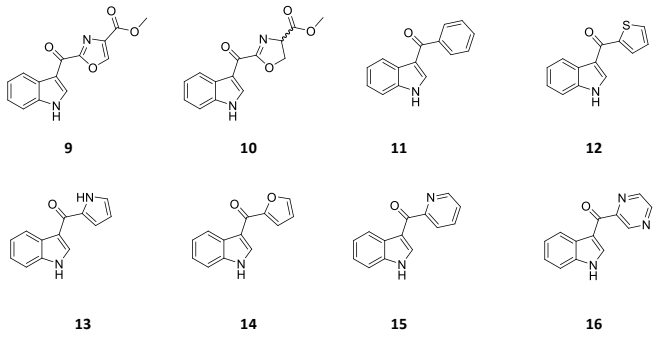

Figure 10. Structure of ITE analogues (**9**-**16**), which have been tested in biologic assays.

Finally, compounds **11**-**16** were designed to further probe π-π stacking interactions with PAS-B AhR, using five- or six-member aromatic groups with different HOMO and LUMO energies (Table 1).

Table 1. Molecular descriptors (cLogP, HOMO, LUMO) calculated for ITE (**7**) and its analogues (**9**-**16**).

Compound	cLogP	HOMO[a]	LUMO[a]
ITE (**7**)	2.15	-0.22042	-0.09203
9	1.60	-0.21720	-0.09443
10	1.53	-	-
11	3.36	-0.21371	-0.07760
12	3.23	-0.21082	-0.07131
13	2.64	-0.21318	-0.06263
14	2.71	-0.20653	-0.07315
15	2.82	-0.20426	-0.07685
16	1.88	-0.21073	-0.09035

[a] Hartree.

Docking studies of compounds **9**-**16** into model **d** of PAS-B AhR support the design strategy, evidencing top scored solutions with similar docked poses to ITE (**7**), and located in an energy window of 2 kcal/mol from the selected binding pose of ITE into model **d** (Figure S8, supplementary material). Compounds **9-16** were then synthesized according to schemes reported in the supplementary material, and tested at 1.0 μM and 0.1 μM concentrations in luciferase transactivation assays. As a result, they do not show any improvement of the transcriptional activity over ITE (**7**), suggesting that each of them loses key interactions to AhR with respect to the parent compound (Figure 11).

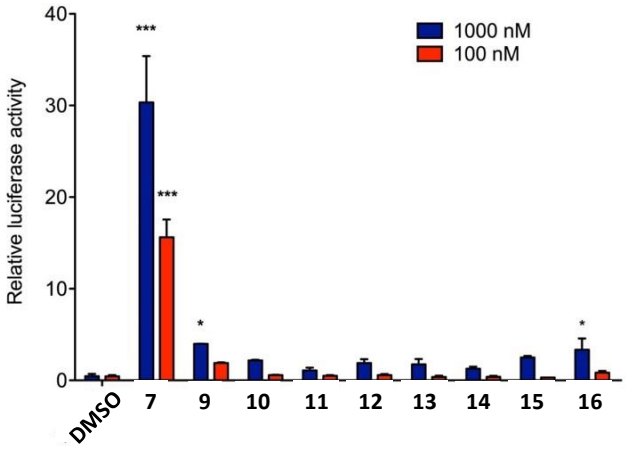

Figure 11. Transactivation activity of AhR by ITE (**7**) and different ITE derivatives (**9**-**16**). Hepatic H1L1 cells were transfected with WT or different AhR mutants: AhR(H285A), AhR(Q377A), AhR(Y316A) or AhR(Y316A/Q377A). After 6 h, cells were lysed, and AhR activation was evaluated by measuring luciferase activity. Data mean ± s.d. of three independent experiments. ***p ≤ 0.001, *p ≤ 0.05, Dunnett test.

In particular, compound **9** is the most active analogue within the series, albeit it shows a drop of transcriptional activity with respect to ITE (**7**). This observation firstly suggests that the increase of ligand hydrophilic property is detrimental for the transcriptional activity. In agreement with mutagenesis data, the lack of activity of compound **10** pinpoints the importance of π-π stacking interactions with His285 and likely Tyr316, whereas a less important role is ascribed to hydrogen bond interactions of the methyl ester moiety. This observation, however, combines with structure activity relationships of compounds **11**-**16** pinpointing how π-π stacking interactions are a necessary but not sufficient condition to bestow potency on ligands. Specifically, the low activity observed for compounds **11**-**16** prompts that removal of the methyl ester group is detrimental for ligand potency. Noteworthy, this observation supports the presence of hydrogen bond interactions between the methyl ester moiety of ITE (**7**) and the backbone atoms of Phe318 and Tyr316. Although these interactions were observed in MD simulations, it is not possible to probe them by mutagenesis experiments given the lack of involvement of side chain atoms. The better activity of compounds **15** and **16** in the series also suggests that the presence of a nitrogen atom as hydrogen bond acceptor group at position 2 of the heteroaromatic ring has a role for activity, supporting the engagement of Tyr316 in hydrogen bond interaction as resulting from the MD study. Conversely, no apparent relationship was found between the activities of compounds **11**-**16** and their relative HOMO and LUMO energies (Table 1).

Taken together, MD simulations, mutagenesis studies and structure-activity relationships of ITE analogues suggest a pharmacophore model of ITE interaction to PAS-B AhR that is composed of the following key structural elements (Figure 12): (i) a first aromatic center located on the thiazole ring (Ar-1; π-π stacking interaction with His285); (ii) one hydrogen bond acceptor

group placed at the carbonyl ester atom (HBA-1; hydrogen bond interaction with Tyr316); (iii) one accessory hydrogen bond acceptor group located at the nitrogen atom of the thiazole ring (HBA-2; hydrogen bond interaction with Tyr316, and Gln377 to a less extend); (iv) a second aromatic center placed on the indole moiety (Ar-2; π-π stacking interaction with Phe316). This pharmacophore model was used to revisit early docking results of ITE (Table S1), looking for additional solutions that could provide alternative binding modes of this ligand to PAS-B AhR. Among alternative binding poses of models **a**-**d** (RMSD > 2.0 Å; Figures S1-S7), none was successful in matching all of the elements of the pharmacophoric model with simultaneous interactions involving key residues His285 and Tyr316, supporting a good performance of the QM/MM-based docking method in this study.

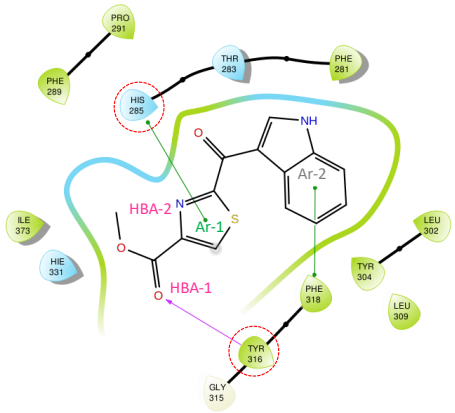

Figure 12. Pharmacophoric model of ITE (**7**) interaction to PAS-B AhR. Key structural elements of ligand are labelled (Ar-1; HBA-1; HBA-2; Ar-2). Key residues of receptor are highlighted with red dashed circles.

Conclusions

AhR is a ligand dependent transcriptional factor involved in the regulation of drug metabolism, inflammation and in several immune functions. ITE (**7**) is an endogenous L-Trp metabolite that potently binds to AhR in the nanomolar range of potency. ITE (**5**) mediated activation of AhR has been associated to immunosuppressive and anticancer functions of the compound. It is also worth noting that, in contrast to other potent AhR ligands such as TCDD (**1**), ITE (**7**) is not endowed with significant AhR mediated toxic effects. The immunoregulatory and anticancer functions of ITE (**7**), combined with its clean toxicological profile, make this endogenous molecule an interesting lead compound for the development of potent and safer AhR agonists for novel therapeutic opportunities in autoimmune disorders and cancer disease. In this paper, we have applied an integrated computational, genetic and synthetic approach to get insights into the binding mode of ITE (**7**) to AhR PAS-B. Results highlighted fingerprint residues of the receptor involved in binding and activity of ITE (**7**), as well as identifying the thiazole ring as key pharmacophoric element of the ligand structure. Collectively, results of docking studies, MD simulations and mutagenesis experiments are consistent with structure–activity relationships obtained from a series of ITE analogues (**9**-**16**), supporting the experimental validity of the proposed binding mode of ITE (**7**) to AhR PAS-B. They pinpoint that π-π stacking interactions rather than hydrophobic contacts, and specific hydrogen bonds of the central heteroaromatic ring and methyl ester moiety are important for ligand binding and potency to AhR, respectively. This information will be instrumental to enable next ITE analogue design and/or structure-based approaches for the development of new AhR modulators on the way to disclose novel immune-regulatory and anticancer therapeutic agents.

Experimental Section

Synthesis. Synthetic methodologies are reported in supplementary material.

*General methods***.** Melting points were determined using a Buchi 535 electrothermal apparatus and are uncorrected. NMR spectra were recorded on a Bruker AC 400 MHz spectrometer in the indicated solvent. Chemical shifts (δ) are reported in parts per million (ppm) and are relative to CD_3OD (3.35 ppm and 49.3 ppm) and d^6-DMSO (2.49 ppm and 39.7 ppm). Coupling constants (*J*) are expressed in Hz. The following abbreviations are used to indicate the multiplicity: s, singlet; d, doublet; dd, doublet of doublets; t, triplet; m, multiplet; brs, broad signal. High resolution mass spectra (HRMS) were recorded on Agilent 6540-UHD Accurate Mass Q-TOF LC/MS instrument. Compounds purity (>95%) was assessed by HPLC analysis (method not validated) using a Shimadzu (Kyoto, Japan) LC-20A Prominence equipped with a CBM-20A communication bus module, two LC-20AD dual piston pumps, a SPD-M20A photodiode array detector and a Rheodyne 7725i injector (Rheodyne Inc., Cotati, CA, USA) with a 20 mL stainless steel loop. A DAD detector was utilized for analysis. The adopted conditions for the analysis were: flow rate 1 mL min^{-1}, a prevail C18 column (250 x 4.6 mm i.d., 5 µm) for compounds **9** and **10**, and a Grace Smart RP18 (250 x 4.6 mm i.d., 5 µm) for compounds **11-16**, using a solution of H_2O/CH_3CN as the eluent. Thin layer chromatography (TLC) was performed in 60 F_{254} (Merck) silica gel supported on aluminium sheets. Spots were visualized by UV detector (λ: 254 nm). Reactions products were purified by flash chromatography on silica gel (Merck 60, 230-400 mesh). ITE (**7**) was purchased from Tocris Biosciences. Reagents were purchased from Sigma Aldrich and Alfa Aesar and were used without further purification. 2-(1'*H*-indol-3'-yl)-2-oxoacetyl chloride (**17**) was prepared according to procedures reported in literature.[27]

(±)-Methyl 2-[2'-(1''*H*-indol-3''-yl)-2'-oxoacetamido]-3-hydroxypropanoate (18).[28] To a stirring suspension of (D, L)-serine methyl ester hydrochloride (2 mmol, 0.31 g) in CH_2Cl_2 (45 mL) at 0 °C, Et_3N (2 mmol, 0.27 mL) was added. After the complete dissolution, 2-(1'*H*-indol-3'-yl)-2-oxoacetyl chloride (**17**) (1.4 mmol, 0.3 g) was added at 0 °C and the resulting solution turns from white to yellow. The mixture was allowed to warm to room temperature and stirred for 12 h. Reaction progress was monitored by TLC (eluent: CH_2Cl_2/MeOH 98:2, v/v). Water (40 mL) was added and the mixture was extracted with CH_2Cl_2 (3 x 10 mL). The combined organic extracts were dried over anhydrous Na_2SO_4 and concentrated under reduced pressure. The crude was purified by flash chromatography on silica gel (eluent: CH_2Cl_2/MeOH 99:1, v/v) affording the title compound (±)-methyl 2-[2'-(1''*H*-indol-3''-yl)-2'-oxoacetamido]-3-hydroxypropanoate (**18**) (460 mg, 1.59 mmol, 80% yield) as a white solid (m.p.: 174-177) ^{1}H NMR (CD_3OD, 400 MHz): δ 8.84 (s, 1H), 8.33-8.35 (m, 1H), 7.50-7.52 (m, 1H), 7.28-7.30 (m, 2H), 4.67 (t, *J*= 3.76 Hz, 1H), 4.05 (dd, J_1= 4.0 Hz, J_2=11.3, 1H), 3.95 (dd, J_1= 3.5, J_2= 11.3 Hz, 1H), 3.82 (s, 3H). ^{13}C NMR (CD_3OD, 100.6 MHz): δ 180.3, 170.4, 163.6, 138.4, 136.5 126.5, 123.5, 122.5, 121.6, 112.5, 111.7, 61.3, 54.6, 51.6. HPLC residence time (t_R): 6.2 min (eluent: H_2O/CH_3CN, 60:40, v/v).

(±)-Methyl 2-(1'*H*-indole-3'-carbonyl)-4,5-dihydrooxazole-4-carboxylate (10).[29] To a suspension of **18** (0.7 mmol, 0.2 g) in freshly distilled CH_2Cl_2 (5 mL), diethylaminosulfurtrifluoride (DAST, 1.5 mmol, 0.2 mL) was added at -78 °C under argon atmosphere. The resulting mixture was allowed to warm to r.t. and stirred for 6 h. Reaction progress was monitored by TLC (eluent: CH_2Cl_2/MeOH 98:2, v/v). Anhydrous K_2CO_3 (0.5 mmol, 0.14 g) was added to reaction mixture. After 30 minutes, the

reaction was poured into aqueous saturated solution of $NaHCO_3$ (20 mL) and the biphasic mixture was extracted with CH_2Cl_2 (3 x 15 mL), dried over anhydrous Na_2SO_4 and concentrated under reduced pressure. The crude was purified by flash chromatography on silica gel (eluent: CH_2Cl_2/MeOH 99:1, v/v) affording the title compound (±)-methyl 2-(1'*H*-indole-3'-carbonyl)-4,5-dihydrooxazole-4-carboxylate (**10**) (130 mg, 0.48 mmol, 69% yield) as a white solid (m.p.: 214-220 °C). ^{1}H NMR (*d*^{6}-DMSO, 400 MHz): δ 12.32 (brs, 1H), 8.59 (s, 1H), 8.19-8.21 (m, 1H), 7.55-7.57 (m, 1H), 7.26-7.32 (m, 2H), 5.12 (dd, J_1= 4.1 Hz, J_2=10.3, 1H), 4.56-4.66 (m, 2H), 3.76 (s, 3H). ^{13}C NMR (CD_3OD, 100.6 MHz): δ 176.4, 171.4, 162.5, 139.1, 137.1, 126.1, 124.2, 123.2, 121.7, 114.4, 113.1, 70.0, 68.7, 52.9. HPLC residence time (t_R): 9.1 min (eluent: H_2O/CH_3CN, 60:40, v/v). FT-IR (KBr): ν 3181, 3077, 2924, 1737, 1605, 1507, 1445, 1380, 1257, 1210, 1033 cm^{-1}. HRMS (ESI) m/z $[M+H]^+$ calcd for $C_{14}H_{13}N_2O_4$ 273.0870; found 273.0882; Δ = 4 ppm.

Methyl 2-(1'*H*-indole-3'-carbonyl)-oxazole-4-carboxylate (9).[30] To a solution of (±)-methyl 2-(1'*H*-indole-3'-carbonyl)-4,5-dihydrooxazole-4-carboxylate (**10**) (0.11 mmol, 0.03 g) in CH_2Cl_2 (25 mL), MnO_2 (1.65 mmol, 0.14 g) was added at room temperature. The resulting suspension was stirred for 3 h at room temperature and then concentrated. Reaction progress was monitored by TLC (eluent: CH_2Cl_2/MeOH 98:2, v/v). The crude was concentrated under reduced pressure and the residue was purified by flash chromatography on silica gel (eluent: CH_2Cl_2/MeOH 99:1, v/v) affording the title compound methyl 2-(1'*H*-indole-3'-carbonyl)-oxazole-4-carboxylate (**7**) (18 mg, 0.067 mmol, 60% yield) as a white solid (m.p.: 250 °C dec.). HPLC residence time (t_R): 14.6 min (eluent: H_2O/CH_3CN, 60:40, v/v). ^{1}H NMR (*d*^{6}-DMSO, 400 MHz): δ 12.37 (br, 1H), 9.12 (s, 1H), 8.91 (s, 1H), 8.28-8.30 (m, 1H), 7.59-7.60 (m, 1H), 7.29-7.31 (m, 2H), 3.89 (s, 3H). ^{13}C NMR (*d*^{6}-DMSO, 100.6 MHz): δ 182.3, 181.9, 170.9, 164.8, 164.5, 139.5, 137.1, 127.0, 124.4, 123.5, 122.1, 113.4, 112.9, 53.2. FT-IR (KBr): ν 3238, 1739, 1608, 1505, 1415, 1231, 1138 cm^{-1}. HRMS (ESI) m/z $[M+H]^+$ calcd for $C_{14}H_{11}N_2O_4$ 271.0713; found 271.0725; Δ = 4 ppm.

General procedure for the synthesis of compounds 11-16.[31] To a mixture of indole (**19**) (1 mmol) in dioxane/AcOH/H_2O (50:20:30, v/v/v, 2 mL mmol^{-1}), $Pd(OAc)_2$ (5 mol%), bipyridine (5 mol%) and the corresponding nitrile derivative (1.2 mmol) were sequentially added and the resulting mixture was stirred at 100 °C for 24 h. The reaction mixture was neutralized by adding aqueous saturated solution of $NaHCO_3$ (20 mL) and extracted with EtOAc (3 x 15 mL). The combined organic extracts were washed with H_2O (20 mL), brine (20 mL), dried over anhydrous Na_2SO_4 and concentrated under reduced pressure. The crude was purified by flash chromatography on silica gel (eluent: *n*-hexane/EtOAc from 100:0 to 60:40, v/v) affording the title compounds **11**-**16**.

(1*H*-indol-3-yl)(phenyl)Methanone (11).[31] The title compound was isolated (49 mg, 0.22 mmol, 22% yield) as brownish solid (m.p.: 168-172 °C). HPLC residence time (t_R): 7.0 min (eluent: H_2O/CH_3CN, 1:1, v/v). ^{1}H NMR (*d*^{6}-DMSO, 400 MHz): δ 12.09 (brs, 1H), 8.25-8.27 (d, *J*=6.84 Hz, 1H), 7.94 (s, 1H), 7.79 (d, *J*=7.5 Hz, 2H), 7.52-7.62 (m, 4H), 7.22-7.28 (m, 2H). ^{13}C NMR (*d*^{6}-DMSO, 100.6 MHz): δ 190.4, 141.0, 137.2, 136.3, 131.5, 128.8 (2x), 126.7, 123.6, 122.4, 121.9, 115.4, 112.7.

(1*H*-indol-3-yl)(thiophen-2-yl)Methanone (12).[32] The title compound was isolated (45 mg, 0.20 mmol, 20% yield) as a white solid (m.p.: 180-182 °C). HPLC residence time (t_R): 11.5 min (eluent: H_2O/CH_3CN, 60:40, v/v). ^{1}H NMR (*d*^{6}-DMSO, 400 MHz): δ 12.14 (brs, 1H), 8.35 (s, 1H), 8.20 (s, 1H), 7.93 (s, 2H), 7.52 (d, *J*= 7.37 Hz, 1H), 7.22-7.26 (m, 3H). ^{13}C NMR (CD_3OD, 100.6 MHz): δ 182.7, 144.9, 137.0, 134.0, 131.6, 131.5, 127.5, 126.4, 123.2, 121.8, 121.4, 115.4, 111.6.

(1*H*-indol-3-yl)(1*H*-pyrrol-2-yl)Methanone (13).[33] The title compound was isolated (15 mg, 0.07 mmol, 7% yield) as a reddish-brownish solid (m.p.: 225-227 °C). HPLC residence time (t_R): 12.9 min (eluent: H_2O/CH_3CN, 70:30, v/v). ^{1}H NMR (*d*^{6}-DMSO, 400 MHz): δ 11.90 (brs, 1H), 11.75 (brs, 1H), 8.22-8.25 (m, 2H), 7.49 (d, *J*= 7.70 Hz, 1H), 7.12-7.23 (m. 2H), 7.07 (s, 1H), 7.01 (s, 1H), 6.22-6.24 (m, 1H). ^{13}C NMR (CD_3OD, 100.6 MHz): δ 180.6, 136.8, 132.2, 132.1, 126.5, 123.8, 122.8, 121.2 (2x), 116.0, 115.5, 111.4, 109.5.

Furan-2-yl(1*H*-indol-3-yl)methanone (14).[33] The title compound was isolated (23 mg, 0.11 mmol, 11% yield) as a white solid (m.p.: 179-182 °C). HPLC residence time (t_R): 8.2 min (eluent: H_2O/CH_3CN, 60:40, v/v). ^{1}H NMR (*d*^{6}-DMSO, 400 MHz): δ 12.14 (brs, 1H), 8.52 (brs, 1H), 8.31 (d, *J*= 7.31 Hz, 1H), 8.00 (s, 1H), 7.53 (d, *J*= 7.82 Hz, 1H), 7.36-7.37 (m, 1H), 7.22-7.26 (m, 2H), 6.74 (s, 1H). ^{13}C NMR (CD_3OD, 100 MHz): δ 177.3, 153.9, 145.7, 136.6, 134.8, 126.6, 123.2, 122.0, 121.6, 116.4, 114.3, 111.7, 111.5.

(1*H*-indol-3-yl)(pyridin-2-yl)Methanone (15).[33] The title compound was isolated (22 mg, 0.10 mmol, 10% yield) as a white solid (m.p.: 188-190 °C). HPLC residence time (t_R): 13.7 min (eluent: H_2O/CH_3CN, 70:30, v/v). ^{1}H NMR (*d*^{6}-DMSO, 400 MHz): δ 12.11 (brs, 1H), 8.82 (s, 1H), 7.62-7.63 (m, 1H), 8.36-8.38 (m, 1H), 8.03-8.05 (m, 2H), 7.61-7.64 (m, 1H), 7.50-7.54 (m, 1H), 7.24-7.27 (m, 2H). ^{13}C NMR (CD_3OD, 100.6 MHz): δ 187.9, 156.7, 148.1, 137.9, 137.3, 136.6, 126.9, 125.7, 123.1, 123.0, 122.1, 121.7, 114.5, 111.5.

(1*H*-indol-3-yl)(pyrazin-2-yl)Methanone (16). The title compound was isolated (20 mg, 0.09 mmol, 9% yield) as a white solid (m.p.: 212 °C dec.). HPLC residence time (t_R): 11.0 min (eluent: H_2O/CH_3CN, 70:30, v/v). ^{1}H NMR (*d*^{6}-DMSO, 400 MHz): δ 12.18 (brs, 1H), 9.15 (brs, 1H), 8.67-8.84 (m, 3H), 8.33 (brs, 1H), 7.52 (brs, 1H), 7.25 (m, 2H). ^{13}C NMR (*d*^{6}-DMSO, 100.6 MHz): δ 185.4, 151.3, 147.2, 144.8, 143.8, 138.6, 136.7, 127.0, 123.8, 122.9, 122.0, 114.2, 112.8.

Molecular Modelling.

Docking Study and Molecular Dynamics. The chemical structures of ITE (**7**) and analogues (**9**-**16**) were generated using *LigPrep 3.2* (Schrödinger, LLC, New York, NY, 2014). For each ligand, we considered different tautomeric and ionization states at the physiological pH of 7.0 ± 2 employing *Epik 3.0* (Schrödinger, LLC, New York, NY, 2014). The geometry of the compounds was refined using DFT/6-31G** calculations with *Jaguar 8.6* (Schrödinger, LLC, New York, NY, 2014).[34] Docking studies into the four models of PAS-B AhR were performed employing the quantum mechanics-polarized ligand docking (QPLD) workflow and *Glide 6.5* (Schrödinger, LLC, New York, NY, 2014).[21] According to this workflow, ligand atomic partial charges are calculated using a QM/MM approach, with the B3LYP method and the 6-31G* basis set, and fitting the electrostatic potential (ESP). Docking study of ITE (**7**) and analogues **9**-**16** were carried out into previously reported homology models of murine PAS-B AhR (models **a**, **b**, **c** and **d** for compound **7**; model **d** for compounds **9**-**16**),[35] employing Glide extra precision mode (XP). The best scored pose of ITE (**7**) obtained by comparing docking solutions among the four in house homology models was selected for multiple molecular dynamic (MD) simulations. Specifically, six MD simulations were carried out using a production time of 50 ns. Briefly, the selected PAS-B AhR ligand bound complex from QPLD docking studies was solvated in an orthorhombic box using TIP3P water molecules, extended 10 Å away from any protein atom. The resulting system was neutralized by adding sodium and chlorine ions at a concentration of 0.15 M. Periodic boundary conditions were applied to avoid finite-size effects. Atomic partial charges of ITE were maintained as obtained from QPLD calculation. MD simulations were performed using *Desmond 4.0* (Schrödinger, LLC, New York, NY, 2014)[28] and the OPLS-2005 force field. The simulation protocol included starting relaxation steps and a final production phase of 50 ns, as previously reported.[20] The occupancy of intermolecular hydrogen bonds, aromatic interactions and hydrophobic contacts was calculated along the last 48 ns of the production phase of each MD simulation, using a cut-off value of 30% and the Simulation Interaction Diagram Tools implemented in *Maestro 10.0* (Schrödinger Release 2014-4: Maestro, Schrödinger, LLC, New York, NY, **2014**).

Molecular Descriptors. Predicted octanol/water partition coefficient (cLogP) was calculated with *QikProp* (Schrödinger Release 2014-4: Maestro, Schrödinger, LLC, New York, NY, 2014), using default options. HOMO and LUMO energies were computed using *Jaguar* (Schrödinger Release 2014-4: Maestro, Schrödinger, LLC, New York, NY, 2014) Single Point Energy (SPE). Hartree Fock theory, accurate level of SCF were employed to calculate Atomic Fukui Indices property.

Biology

Mouse embryonic fibroblast derivation. The mouse embryonic fibroblasts (MEFs) were obtained according to the guidelines of University of Perugia Ethical Committee and the European Communities Council Directive 2010/63/EU. MEFs and AhR−/− MEFs were prepared respectively from C57BL/6 mice and AhR −/− C57BL/6 mice, and the preparation protocol was adapted from J. Xu.[36] The pregnant mice were sacrificed at 13,5 d.p.c. (day post-coitum) by cervical dislocation. 5–7 embryos can be expected from each pregnant female, and they should yield enough MEFs for several experiments. The embryos were separated from placenta and membranes and placed in 10-cm culture dishes in sterile PBS 1X. Then liver, heart and brain were removed and discarded. The remaining part of each embryos were washed and minced with cool razor blades and incubated 20 minutes at 37°C with trypsin-EDTA 500 mg/L. The minced tissues were chopped by repeated pipetting, then cell suspension were plate in 10-cm tissue culture dishes and 10 ml of DMEM medium containing 10% FBS (Euroclone) were added. Electroporation was used to transfect MEFs.

AhR Mutagenesis. PEZ-M02 containing murine AhR was used as templates for in vitro expression of the AhR.[37] Mutation of selected amino acids within the AhR to alanine (H285A, Y316A, Q377A), was carried out using specific primers containing the specific mutation.

AhR H285A:

5'-TCTTCAGGACCAAAGCCAAGCTAGACTTCA-3'

5'-TGAAGTCTAGCTTGGCTTTGGTCCTGAAGA-3'

AhR Y316A:

5'-CAAGAGGATCGGGGGCCCAGTTCATCCATG-3'

5'-CATGGATGAACTGGGCCCCCGATCCTCTTG-3'

AhR Q377A:

5' - ATC ATC GCC ACT GCG AGA CCA CTG -3'

5'- CAG TGG TCT CGC AGT GGC GAT GAT -3'

Luciferase Assay of AhR Mutants. AhR-deficient mouse embrional fibrobasts (MEF) (2x105) were electroporated (230 V, 75 Ohm and 1,500 microfarads) with: (2ug) of WT or each of AhR mutant (H285A), (Q377A), (Y316A), in Optimem/Glutamax (Invitrogen) in combination with 0,8 µg of the firefly luciferase reporter pGudLuc1.1 plasmid, which contains a 480 bp fragment of the upstream enhancer region of the mouse Cyp1a1 gene – including four xenobiotic response elements – upstream of the firefly luciferase coding sequence. Another reporter plasmid, pRL-TK (0,2 µg; Promega) encoding Renilla luciferase, was electroporated as an internal control of the transfection process. Cells were seeded in 24-well plates at a density of 2 × 105 cells/ml. After 24 h at 37 °C, cells were stimulated for 6h with specific concentrations of ITE or its derivatives. Luciferase assays were performed using the dual luciferase reporter assay kit (Promega).

Supporting Information: Table S1. Top ten ranked poses of ITE (**7**) into the homology models **a**-**d** of PAS-B AhR; Table S2**.** Root mean square fluctuations (RMSF, Å) of residues lying in a 3Å shell around ITE (**7**); Table S3**.** Occupancy values (mean ± standard deviation) of interactions observed in the six MD trajectories between ITE (**7**) and binding site residues; Figure S1. Interaction plots of top scored binding poses of ITE (**7**) in models **a**-**d**; Figures S2-S7. Interaction plots of other scored binding poses of ITE (**7**) in models **a**-**d** showing RMSD > 2.0Å; Figure S8. Top scored binding poses of ITE analogues (**9**-**16**) as docked into model **d**, and superimposed to the top scored binding pose ITE (**7**) in model **d**; Synthetic methodologies; Spectroscopic and analytical characterization of compounds **9**-**16**, **18**.

Acknowledgements

This study was also supported by Telethon Research Grant GGP14042 to F.F.

Keywords: Immunotherapy • Cancer • Tryptophan • AhR • ITE

References:

[1] T. V. Beischalg, J. L. Morales, B. D. Hollinshead, G. H. Perdew, *Crit. Rev. Eukaryot. Gene Expr.* **2008**, *18*, 207-250.

[2] E. Guyot, A. Chevallier, R. Barouki, X. Coumoul, *Drug Discov. Today*, **2013**, *18*, 479-486.

[3] Y. Cheng, U.H. Jin, L.A. Davidson, R.S. Chapkin, A. Jayaraman, P. Tamamis, A. Orr, C. Allred, M.S. Denison, A. Soshilov, E. Weaver, S. Safe, Toxicol. Sci., **2017**, *155*, 458-473.

[4] L. P. Nguyen, C. A. Bradfield, *Chem. Res. Toxicol.* **2008**, *21*, 102-116.

[5] J. D. Mezrich, J. H. Fechner, X. Zhang, W. J. Burlingham, C. A. Bradfield, *J. Immunol.* **2010**, *185*, 3190-3198.

[6] J. Song, M. Clagett-Dame, R. E. Peterson, M. E. Hahn, W. E. Westler, R. R. Sicinski, H. F. DeLuca, *Prot. Natl. App. Sci. USA*, **2002**, *99*, 14694-14699.

[7] G. Gaitanis, P. Magiatis, K. Stathopoulou, I.D. Bassukas, E.C. Alexopoulos, A. Velegraki, A.L. Skaltsounis, *J. Invest. Dermatol.*, **2008**, *128*, 1620-1625.

[8] F. J. Quintana, G. Murugaiyan, M. F. Farez, M. Mitsdoerffer, A. M. Tukpah, E. J. Burns, H. L. Weiner, *Proc. Natl. Acad. Sci. USA*, **2010,** *107*(48), 20768-20773.

[9] L. F. Nugent, G. Shi, B. P. Vistica, O. Ogbeifun, S. J. H. Hinshaw, I. Gery, *Invest. Ophthalmol. Vis. Sci.* **2013**, *54*, 7463-7469.

[10] C. Wang, Z. Ye, A. Kijlstra, Y. Zhou, P. Yang, *Clin. Exp. Immunol.* **2014**, *177*, 521-530.

[11] P. Wei, G. H. Hu, H. Y. Kang, H. B. Yao, W. Kou, H. Liu, C. Zhang, S. L. Hong, *Lab. Invest.* **2014**, *94*, 528-535.

[12] T. Yoshida, K. Katsuya, T. Oka, S. Koizumi, D. Wakita, H. Kitamura, T. Nishimura, *Biomed. Res.* **2012**, *33*, 67-74.

[13] K. Wang, Y. Li, Y. Z. Jiang, C. F. Dai, M. S. Patankar, J. S. Song, J. Zheng, *Cancer Lett.* **2012**, *340*, 63-71.

[14] J. Cheng, W. Li, B. Kang, Y. Zhou, J. Song, S. Dan, Y. Yang, X. Zhang, J. Li, S. Yin, H. Cao, H. Yao, C. Zhu, W. Yi, Q. Zhao, X. Xu, M. Zheng, S. Zheng, L. Li, B. Shen, Y. J. Wang, *Nat. Commun.* **2015**, *6*, 7209-7221.

[15] E. C. Henry, J. C. Bemis, O. Henry, A. S. Kende, T. A. Gasiewicz, *Arch. Biochem. Biophys.* **2006**, *450*, 67-77.

[16] Y. Wu, X. Chen, Q. Zhou, Q. He, J. Kang, J. Zheng, K. Wang, T. Duan, *PLoS One*, **2014**, *9*, e86549.

[17] E. C. Henry, S. L. Welle, T. A. Gasiewicz, *Toxicol. Sci.* **2010**, *114*(1), 90-100.

[18] A. Perkins, J. L. Phillips, N. I. Kerkvliet, R. L. Tanguay, G. H. Perdew, S. K. Kolluri, W. H. Bisson, *Biology (Basel)*, **2014**, 3, 645-669.

[19] W. H. Bisson, D. C. Koch, E. F. O'Donnell, S. M. Khalil, N. I. Kerkvliet, R. L. Tanguay, R. Abagyan, S. K. Kolluri, *J. Med. Chem.* **2009**, 52, 5635-5641.

[20] R. Nuti, M. Gargaro, D. Matino, D. Dolciami, U. Grhomann, P. Puccetti, F. Fallarino, A. Macchiarulo, *J. Chem. Inf. Model,* **2014**, *54*, 3373-3383.
[21] A. E. Cho, V. Guallar, B. Berne, R. A. Friesner, *J. Comput. Chem.*, **2005**, *26*, 915-931.
[22] G.L. Warren, C.W. Andrews, A.M. Capelli, B. Clarke, J. LaLonde, M.H. Lambert, M. Lindvall, N. Nevins, S.F. Semus, S. Senger, G. Tedesco, I.D. Wall, J.M. Woolven, C.E. Peishoff, M.S. Head, *J. Med. Chem.*, **2006**, 49, 5912-5931.
[23] A. Crespo, A. Rodriguez-Granillo, V.T. Lim, *Curr. Top. Med. Chem*. **2017**, *17*, 2663-2680.
[24] J.Y. Chung, J.M Hah, A.E. Cho, J. Chem. Inf. Model. **2009**, *49*, 2382-2387.
[25] A.E. Cho, J.Y. Chung, M. Kim, K. Park, *J. Chem. Phys*. **2009**, 131, 134108.
[26] G.N. Winston-McPherson, D. Shu, W. Tang, *Bioorg. Med. Chem. Lett.*, **2014**, 24, 4023-4025
[27] M. Mielczarek, R. V. Devakaram, C. Ma, X. Yang, H. Kandemir, B. Purwono, D. S. C. Black, R. Griffith, P. J. Lewis, N. Kumar, *Org. Biomol. Chem.* **2014**, *12*, 2882-2894.
[28] D. H. Dethe, A. Ranjan, V. H. Pardeshi, *Org. Biomol. Chem.* **2011**, *9*, 7990-7992.
[29] A. J. Phillips, Y. Uto, P. Wipf, M. J. Reno, D. R. Williams, *Org. Lett.* **2000**, *2*, 1165-1168.
[30] P. K. Grzywacz, R. R. Sicinski, H. F. DeLuca, *Heterocycles*, **2003**, *60*, 1219-1224.
[31] T. Das, A. Chakraborty, A. Sarkar, *Tetrahedron Lett.* **2014**, *55*, 7198-7202.
[32] J. H. Wynne, C. T. Lloyda, S. D. Jensena, S. Bosonb, W. M. Stalick, *Synthesis*, **2004**, *14*, 2277-2282.
[33] A. R. Katritzky, K. Suzuki, S. K. Singh, H. Y. He, *J. Org. Chem.* **2003**, *68*, 5720–5723.
[34] A. D. Bochevarov, E. Harder, T. F. Hughes, J. R. Greenwood, D. A. Braden, D. M. Philipp, D. Rinaldo, M. D. Halls, J. Zhang, R. A. Friesner, *Int. J. Quantum Chem.*, **2013**, *113*, 2110-2142.
[35] D. Shivakumar, J. Williams, J., Wu, Y., Damm, W., Shelley, J., Sherman, W., *J. Chem. Theory Comput.*, **2010**, *6*, 1509-1519.
[36] J. Xu, *Curr. Prot. Mol. Biol.* **2005**, *Chapter 28*, Unit 21.
[37] A. Bessede, M. Gargaro, M. T. Pallotta, D. Matino, G. Servillo, C. Brunacci, S. Bicciato, E. M. Mazza, A. Macchiarulo, C. Vacca, R. Iannitti, L. Tissi, C. Volpi, M. L. Belladonna, C. Orabona, R. Bianchi, T. V. Lanz, M. Platten, M. A. Della Fazia, D. Piobbico, T. Zelante, H. Funakoshi, T. Nakamura, D. Gilot, M. S. Denison, G. J. Guillemin, J. B. DuHadaway, G. C. Prendergast, R. Metz, M. Geffard, L. Boon, M. Pirro, A. Iorio, B. Veyret, L. Romani, U. Grohmann, F. Fallarino, P. Puccetti. *Nature*, **2014**, *511*, 184-219.

Entry for the Table of Contents

Insert graphic for Table of Contents here.

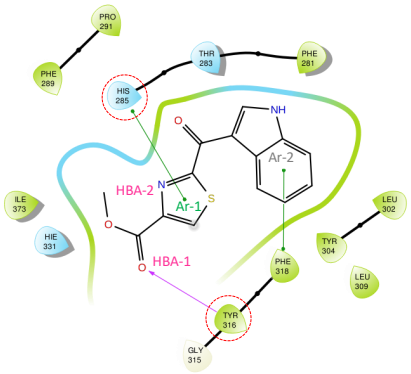

ITE is an endogenous product of L-Tryptophan catabolism. It is also a non-toxic AhR agonist endowed with immunomodulatory properties. In this study, we used docking and molecular dynamics to investigate the binding mode of ITE into the ligand binding pocket of AhR. Mutagenesis studies were instrumental to validate the proposed binding mode, identifying His285 and Tyr316 as key residues for ligand-dependent receptor activation. ITE analogues were also synthesized to develop a pharmacophoric model of relevant interactions to AhR.